Growing Critical: Self-Organized Criticality in a Developing Neural System

Felipe Yaroslav Kalle Kossio,[1] Sven Goedeke,[1] Benjamin van
den Akker,[2] Borja Ibarz,[3] and Raoul-Martin Memmesheimer[1, 2]

[1] *Neural Network Dynamics and Computation, Institute of Genetics, University of Bonn, Bonn, Germany*
[2] *Department of Neuroinformatics, Radboud University Nijmegen, Nijmegen, Netherlands*
[3] *Nonlinear Dynamics and Chaos Group, Departamento de Fisica, Universidad Rey Juan Carlos, Madrid, Spain*

Experiments in various neural systems found avalanches: bursts of activity with characteristics typical for critical dynamics. A possible explanation for their occurrence is an underlying network that self-organizes into a critical state. We propose a simple spiking model for developing neural networks, showing how these may "grow into" criticality. Avalanches generated by our model correspond to clusters of widely applied Hawkes processes. We analytically derive the cluster size and duration distributions and find that they agree with those of experimentally observed neuronal avalanches.

Keywords: Neural networks, Hawkes processes, network growth, self-organized criticality, avalanches

Introduction.—A hallmark of systems at criticality is the variability of their responses to small perturbations. While small responses are most likely, the probability of large, system-size effects is non-negligible. Various natural and model complex systems show similar behavior [1]. One explanation is that they drive themselves close to a critical state ("self-organized criticality" [2, 3]). The dynamics of such systems are characterized by "events" or "avalanches". Their sizes and durations follow power-law distributions, frequently with exponents 3/2 and 2, indicating an underlying critical branching process [4–7]. Apparent critical dynamics, "neuronal avalanches", in biological neural networks were first reported in Refs. [8, 9]. It has been suggested that they foster information storage and transfer [10, 11]. Experimental studies often report power-law size and duration distributions with exponents 3/2 and 2. They further indicate that neuronal avalanches emerge during development [12–15], suggesting that neural networks develop into a critical state.

The development of neural networks is determined by an interplay of genetic determinants and environmental influence. Of pivotal importance is neural activity [16, 17]. As a general rule, neurons with low activity level extend their neurites and form more activating connections, while highly active cells reduce these [18–20]. Thereby, neurons maintain their average activity at a particular level (homeostasis) [21–23].

Computational models for avalanches in neural systems rely on static, tuned connectivity [14, 24], on short-term synaptic plasticity [25, 26], or on long-term network changes [27–30]. Here we propose a continuous-time spiking neural network model belonging to the third class. The avalanche dynamics follow from a network growth process towards a critical state, which uses local information only [31–33]. The model is rooted in previous models for neural network development [27, 29, 34], but sufficiently simple to be analytically tractable.

Neuron model.—Like biological neurons, our model neurons communicate by sending and receiving spikes in continuous time. Spiking is stochastic, according to an inhomogeneous Poisson point process with instantaneous rate $f_i(t)$ for neuron i [27, 35–38]. In isolation neurons have a low spontaneous rate f_0, e.g., due to spontaneous synaptic release or channel fluctuations [39, 40]. A spike from neuron j increases f_i by the size of the time-dependent connection strength gA_{ij}. The increment decays exponentially with time constant τ, which accounts for relaxation due to leak currents. The couplings are excitatory; this is the dominant connection type in developing neural systems [34]. Taken together, f_i's dynamics follow

$$\tau \dot{f}_i(t) = f_0 - f_i(t) + \tau g \sum_j A_{ij}(t^-) \sum_{\hat{t}_j} \delta\left(t - \hat{t}_j\right), \quad (1)$$

where $\hat{t}_j$ denotes the spike times of neuron j (δ is the Dirac delta distribution). For simplicity, we assume that all neurons have the same parameters. For constant couplings, the network dynamics form a multivariate Hawkes point process [37, 38, 41].

Network growth.—Neurons are commonly arranged in single or stacked layers. We thus represent neurite extents by disks with radii $R_i(t)$, with centers, representing cell somas, randomly and uniformly distributed in a planar area [27, 34, 42]. Since neurons with more neurite overlap can grow more synaptic connections [43, 44], connection strengths are set proportional to the overlap areas $A_{ij}(t)$ of the disks, with proportionality constant g. We incorporate homeostatic neurite growth by evolving extents as

$$\dot{R}_i(t) = K \left(1 - \frac{1}{f_{\text{sat}}} \sum_{\hat{t}_i} \delta(t - \hat{t}_i) \right), \quad (2)$$

Fig. 1. Between spikes of neuron i, $R_i(t)$ grows linearly with rate K. At spike sending, it shrinks by a constant amount K/f_{sat}, which determines the rate f_{sat} at which growth and shrinkage equilibrate. There are no self-connections. Growth takes much longer than decay of activity, $1/K \gg \tau$ (spatial scales of the population are
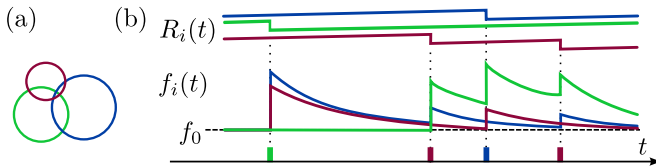
FIG. 1. Neuron dynamics. (a) Neurons' somas and neurite extents are represented by disks with evolving radii. Coupling strengths are proportional to neurite overlap areas. (b) Neurite radii increase linearly (upper traces), own spike sendings (lower trace) result in instantaneous shrinkage. Spike arrivals increase the instantaneous firing rate by the coupling strength, it decays exponentially in between (middle trace).
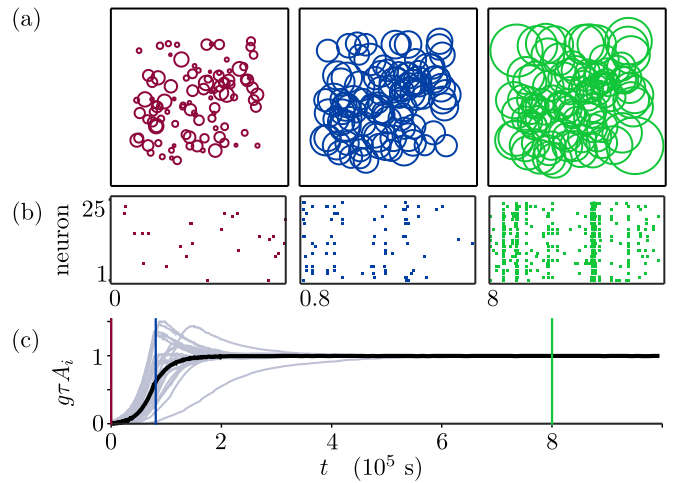

FIG. 2. Network dynamics. (a) Extents of neurites. (b) Spikes generated by 25 sample neurons (100 s windows). (c) Scaled total overlaps of 25 sample neurons (gray) and the population average (black) as a function of time. For (a) and (b) from left to right: initial state (red), state with growth on average (blue), stationary state (green). Color coded vertical lines in (c) indicate the three different time points in (a) and (b).

of order one). Furthermore, we assume $f_{\mathrm{sat}} \gg f_0$, in agreement with experiments [15, 40, 45]. Spontaneously inactive neurons would reduce the relevant average f_0 [45]. The growth model is biologically inspired; it is a simplification of previous growth models [23, 27, 29, 34]. However, many slow homeostatic processes [21, 22, 48] with $f_{\mathrm{sat}} \gg f_0$ will yield similar results.

The neurons are initially mostly isolated. Over time, they extend their neurites, form connections, and develop a network, Fig. 2. At intermediate stages, neurites and overlaps can overshoot [15, 29, 34]. When neuron i's time-averaged firing rate $\bar{f}_i$ reaches f_{sat}, its average growth stops [Eq. (2)]. Our networks grow into a stationary state, where $\bar{f}_i = f_{\mathrm{sat}}$ for all i. In the following, we investigate this state.

Stationary state dynamics.—We first compute the average number of spikes that a spike directly causes: Identical $\bar{f}_i$ imply identical time-averaged total overlaps $\sum_j \bar{A}_{ij} = \bar{A}_i = \bar{A}$ and input coupling strengths. Time averaging Eq. (1), $\bar{f}_i = f_0 + \tau g \sum_j \bar{A}_{ij} \bar{f}_j$ [here and henceforth we neglect the small fluctuations of $A_{ij}(t)$ around $\bar{A}_{ij}$], and inserting f_{sat} yields $\tau g \bar{A} = 1 - f_0/f_{\mathrm{sat}}$. A spike of neuron j at $\hat{t}_j$ adds $g A_{ij}(\hat{t}_j^-) e^{-(t-\hat{t}_j)/\tau} \Theta(t-\hat{t}_j)$ to $f_i(t)$ [Eq. (1), Θ is the Heaviside function], such that the number of additionally induced spikes in neuron i is Poisson distributed with mean $\tau g A_{ij}(\hat{t}_j^-)$. Averaged over the randomness of spike generation each spike thus generates in total

$$\sigma = \tau g \sum_i \bar{A}_{ij} = \tau g \bar{A} = 1 - \frac{f_0}{f_{\mathrm{sat}}} \qquad (3)$$

spikes, where we used the symmetry of overlaps, $A_{ij} = A_{ji}$, $\sum_i \bar{A}_{ij} = \sum_j \bar{A}_{ij} = \bar{A}$. Equation (3) holds independently of network activity and neuron identity, due to the linearity of Eq. (1) and the homogeneity of parameters. In particular, σ equals also the time and population average number of induced spikes ($\propto f_{\mathrm{sat}} - f_0$) per spike ($\propto f_{\mathrm{sat}}$).

The independence of spike offspring generation from other spikes allows us to understand the dynamics as a branching process with branching parameter σ. More specifically, we have an age-dependent or Crump-Mode-

Jagers branching process [49]: Individuals (spikes) generate offspring at an age-dependent rate. Neuronal avalanches are trees of offspring, started by a spontaneous spike. For their overall size only the distribution of single spike offspring matters. It is Poissonian with parameter σ. The avalanche sizes s therefore follow the Borel distribution [50],

$$P(s) = \frac{(s\sigma)^{s-1} e^{-s\sigma}}{s!}. \qquad (4)$$

We apply Stirling's approximation to obtain

$$P_{\mathrm{appr}}(s) = \frac{1}{\sqrt{2\pi\sigma}} s^{-3/2} e^{-(\sigma - \ln\sigma - 1)s}, \qquad (5)$$

explicitly highlighting the power-law tail with exponent $3/2$ of a critical branching process for $\sigma = 1$ [4–7]. For a subcritical process ($\sigma < 1$), Eq. (5) is a power law with exponential cutoff around $s_c(\sigma) = (\sigma - \ln\sigma - 1)^{-1}$. It signifies subcritical dynamics [4, 5, 51], not a finite size effect [3, 5]; the size distribution is independent of neuron number. Equation (5) inherits the good quality of Stirling's approximation [52], with relative error about $1/(12s)$.

The heights of Crump-Mode-Jagers trees, i.e., the temporal differences T between their first and last individuals, represent the durations of the corresponding neuronal avalanches. In the following we derive their probability density $p(T)$. Because of the additivity of Poisson processes, the superposition of all neurons' spike trains can be described as an inhomogeneous Poisson process with rate $f(t) = \sum_i f_i(t)$. Summing
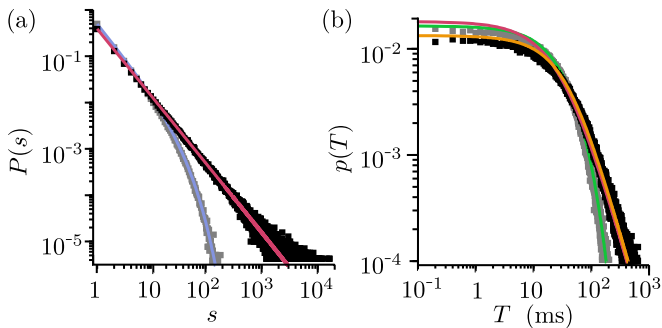
FIG. 3. Avalanche sizes and durations. (a) Analytical size distributions Eq. (5) (discrete points connected) and simulation results for subcritical ($f_{\rm sat} = 0.04\,$Hz, $\sigma = 0.75$, $t_{\rm bin} = 30\,$ms, blue and gray) and near-critical ($f_{\rm sat} = 2\,$Hz, $\sigma = 0.995$, $t_{\rm bin} = 45\,$ms, red and black) states. Equation (4) yields visually indistinguishable analytics. (b) Analytical duration distributions Eq. (10) and simulation results, for subcritical (green and gray) and near-critical (orange and black) states, and closed-form approximation Eq. (12) (red).

Eq. (1) over i and inserting $\bar{A} = \sigma/(g\tau)$ [Eq. (3)] yields $\tau \dot{f}(t) = Nf_0 - f(t) + \sigma \sum_{\hat{t}} \delta(t - \hat{t})$ with the number of neurons N. $\hat{t}$ are the neurons' spike times; they occur with instantaneous rate $f(t)$. The spiking dynamics may thus be interpreted as a self-exciting Hawkes process. It is Markovian due to the exponentially decaying impact kernel [53, 54]. The spontaneous background rate Nf_0 initiates avalanches. To determine their durations, we consider an analogous process with instantaneous rate $f_a(t)$ and without spontaneous spiking, which is initiated at $t = 0$ by an external spike,

$$\tau \dot{f}_a(t) = -f_a(t) + \sigma \sum_{\hat{t}_a} \delta(t - \hat{t}_a), \ f_a(0) = \frac{\sigma}{\tau}. \qquad (6)$$

The duration of an avalanche is the time T of this process' last spike. The probability that it has occurred before t gives the distribution function $P(T \leq t)$ of durations. We first compute this probability conditioned on the instantaneous rate $f_a(t)$ at the end of the considered interval:

$$\begin{aligned} P(T \leq t \mid f_a(t)) &= P(\text{no spike in } (t, \infty) \mid f_a(t)) \\ &= e^{-\int_t^\infty f_a(t')dt'} = e^{-\tau f_a(t)}, \end{aligned} \qquad (7)$$

where we use that the process behaves like a Poisson process with exponentially decaying rate, if no spike is generated. Averaging over $f_a(t)$ yields

$$\begin{aligned} P(T \leq t) &= \int_0^\infty P(T \leq t \mid f_a(t)) \, p(f_a(t)) \, df_a(t) \\ &= E(e^{-\tau f_a(t)}). \end{aligned} \qquad (8)$$

$E(\cdot)$ denotes the expectation value over the process, Eq. (6). Importantly, Eq. (8) shows that $P(T \leq t)$ equals

the Laplace transform of the random variable $f_a(t)$, evaluated at the decay time τ. This Laplace transform has recently been derived [55–57]. Inserting our parameters yields $E(e^{-\tau f_a(t)}) = e^{\sigma a(t)/\tau}$, where $a(t)$ satisfies

$$\dot{a}(t) = -a(t)/\tau + e^{\sigma a(t)/\tau} - 1, \ a(0) = -\tau. \qquad (9)$$

The resulting $P(T \leq t) = e^{\sigma a(t)/\tau}\Theta(t)$ with $\Theta(0) = 1$ has the density

$$p(T) = \sigma\dot{a}(T)e^{\sigma a(T)/\tau}\Theta(T)/\tau + e^{-\sigma}\delta(T). \qquad (10)$$

We can generalize Eq. (9) to Hawkes processes with different kernels using the integral equation for cluster duration distributions [58, 59].

We finally approximate $p(T)$ by closed-form expressions with a focus on its tail near criticality. For large t, $P(T \leq t)$ approaches 1, so $a(t)$ approaches 0. Generally, $\sigma a(t)/\tau$ stays between -1 and 0. Expanding $e^{\sigma a(t)/\tau}$ in Eq. (9) around $\sigma a(t)/\tau = 0$ to second order,

$$\dot{a}(t) \approx (\sigma - 1)a(t)/\tau + \sigma^2 a(t)^2/(2\tau^2), \ a(0) = -\tau, \qquad (11)$$

yields closed-form approximations for $a(t)$. In particular, for nearly critical systems with $\sigma \approx 1$, the first term on the right-hand side vanishes and the solution is $a_{\rm appr}(t) = -2\tau^2/(2\tau + t)$, leading to a probability density

$$p_{\rm appr}(T) = 2\tau(2\tau+T)^{-2}e^{a_{\rm appr}(T)/\tau}\Theta(T)+e^{-1}\delta(T), \qquad (12)$$

which approaches for large T a power law with critical exponent 2. For large t the error in the expansion Eq. (11) becomes negligible, $a_{\rm appr}(t)$ thus has the right slope and $p_{\rm appr}(T)$ equals $p(T)$ up to a factor (Fig. 3). We conclude that the duration distribution has a power-law tail with critical exponent 2. Expanding the exponential to third order yields a closed-form distribution that is a good approximation also for small T.

Simulations.—We complement our analytics with simulations to (i) compare the avalanche distributions, (ii) exemplify the irrelevance of connectivity fluctuations, (iii) investigate the spatial spread of avalanches, (iv) address the robustness of the results, and (v) consider a typical experimental manipulation. If not stated otherwise, $N = 100$, $\tau = 10\,$ms [60], $g = 500\,$Hz, $f_0 = 0.01\,$Hz, $f_{\rm sat} = 2\,$Hz [15, 40], somas are placed on unit square, $K^{-1} = 10^6\,$s (quick growth, accelerating simulations) [15, 21, 22, 29]. The simulations use an event-based algorithm. Next spike times are determined using inverse transform sampling of the interspike-interval distribution; we avoid nonelementary functions by splitting each neuron's Poisson process into a homogeneous (rate f_0) and an inhomogeneous one.

An avalanche should be a sequence of offspring spikes of one spontaneous progenitor. To keep contact with the experimental literature, we analyze numerical data by binning time and considering spike sequences that are not separated by an empty bin as one avalanche [8, 61–63]. Our model yields analytical estimates for

the probabilities that binning splits the first avalanche spikes or merges them with the next avalanche, as well as for splitting or merging an average avalanche. Keeping them moderate provides our bin sizes t_{bin} in terms of experimentally accessible quantities $(f_0, \tau, N, f_{\text{sat}})$ [45]. Results are robust against changing t_{bin}.

(i) In all simulations the model reaches a stationary state. The avalanche distributions agree well with the analytically derived ones, Fig. 3, the effects of binning and avalanche overlaps are small. We quantitatively test this agreement using the methods described in Refs. [64, 65]. For both size and duration distributions a pure power law is ruled out, as expected. For the size distribution, a power law with exponential cutoff, cf. Eq. (5), yields a good fit. The analytical values of the power-law exponent, the cutoff $s_c(\sigma)$, and the resulting σ are closely matched.

(ii) The fluctuations of $\sum_j A_{ij}(t)$ and the deviations of $\bar{f}_i$ from f_{sat} are small ($< 1\%$, Fig. 2). Freezing the network ($K = 0$) in the stationary state has no effect on the avalanche statistics: Neuronal growth carries the system close to a critical point, but is not required later on. This is in agreement with self-organized criticality and excludes other mechanisms [66–68].

(iii) To investigate spatial spread near criticality, we compute covariances $C_{ij} = \langle n_i n_j \rangle - \langle n_i \rangle \langle n_j \rangle$ between numbers n_i, n_j of spikes contributed to single avalanches by neurons i, j with various distances. Covariances decay comparably slowly. Covariances and thus avalanches spread beyond direct connections, Fig. 4(a).

(iv) To test robustness, we first freeze the growth in the stationary state and shuffle the output vectors (columns of the coupling matrix) between neurons. While this alters the network topology and breaks coupling symmetry, it leaves the essential total coupling strengths unchanged. Indeed, we observe little effect on avalanche sizes and durations. Second, we consider moderate nonadditivity of spike impacts. We introduce an absolute refractory period τ_{ref} after a sent spike, during which the neuron cannot spike again. We observe that although the refractory period limits the firing rate, the network reaches a stationary state with the same average individual rate f_{sat} as before: larger overlaps compensate refractoriness. For a refractory period about τ, which is often biologically plausible [39, 60], the statistics resemble the original one for small and medium size avalanches [Fig. 4(b), red vs. gray]. Larger couplings and stop of avalanches lacking available neurons cause an excess of larger avalanches, followed by a strong reduction. Neurons still frequently contribute several spikes to avalanches. With long refractoriness, little similarity remains [Fig. 4(b), green and blue; blue: our model with parameters adapted from Ref. [27], calcium variable present in Ref. [27] does not affect distribution shape].

(v) Manipulation of neural excitability or coupling strength via g causes subcriticality (decreased g) or ex-
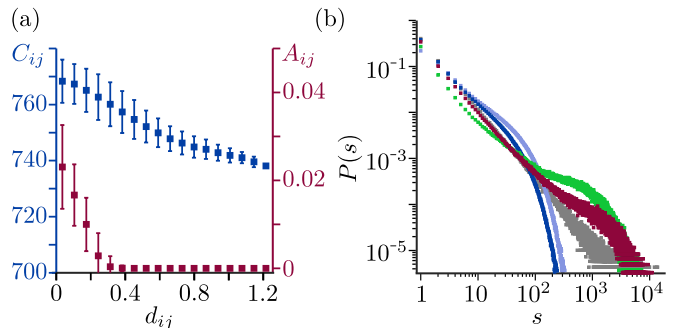

FIG. 4. (a) Pairwise spike number covariances and overlaps as functions of the intersomatic distances d_{ij} (averages around a particular intersomatic distance, bars: standard deviations), $\sigma = 0.995$, $t_{\text{bin}} = 45\,\text{ms}$. (b) Avalanche size distributions for the same model as in Fig. 3, but with absolute refractory period $\tau_{\text{ref}} = \tau$ (red), $\tau_{\text{ref}} = 4\tau$ (green), $\tau_{\text{ref}} = 0\,\text{ms}$ (gray) for reference, $t_{\text{bin}} = 45\,\text{ms}$; $\tau = 5\,\text{ms}$, $\tau_{\text{ref}} = 4\tau$, $f_0 = 0.1\,\text{Hz}$, $f_{\text{sat}} = 0.8\,\text{Hz}$, $t_{\text{bin}} = 10\,\text{ms}$ (blue, $t_{\text{bin}} = 45\,\text{ms}$: light blue).

cess of large avalanches (increased g), as in experiments [8, 69]. Our model predicts that the latter is balanced by network plasticity faster than the former, due to strongly increased activity [45].

Discussion and conclusion.—We suggest an analytically tractable model for neural network growth, which may explain the emergence of subcritical and critical avalanche dynamics. It covers essential features of biological neurons such as operation in continuous time, spiking, leak currents, and network growth. Still, it allows the analytical computation of the avalanche size and duration distributions for subcritical and critical stationary states. Our numerical analysis confirms their validity and robustness and yields additional insight.

Two features are responsible for the emergence of the (near-)critical state (Fig. 3): (i) homeostatic growth to attain a saturation rate that is high compared to the spontaneous one (precise values of f_{sat} and f_0 are irrelevant), and (ii) linear summation of spike impacts. (i) implies that in the stationary state on average each spike generates nearly one successor. This holds for all networks with largely self-sustained activity. Usually, however, branching parameters vary, for example at high network activity spikes generate less offspring. This drives activity excursions back and generates non-power-law distributions [70, 71]. In our networks, (ii) implies that the branching parameter is the same for each spike. Small saturation rates yield subcritical dynamics (Fig. 3), strong nonlinearities other deviations [Fig. 4(b)]. Our model thus predicts that neural networks may develop criticality already due to their growth, that spontaneous spiking in such networks is low compared to saturation, and that spike effects add rather linearly and are independent of activity level. For example, starburst amacrine cells have radial dendritic trees, interact during development via

dendro-dendritic excitatory connections and are reported to generate critical avalanches [14]. Our model predicts that higher precision measurements will reveal deviations as in Fig. 4(b), due to the cells' long refractory periods.

Our network model is based on the neurobiologically more detailed ones [27, 29, 34]. Motivated by experiments, Ref. [34] proposes radial activity dependent neurite outgrowth steered by calcium dynamics and finds convergence to a stationary state for certain parameter ranges. To study avalanches, Ref. [27] adds stochastically spiking neurons, albeit with long refractoriness and larger f_0/f_{sat}, impeding analytical treatment and causing large deviations from criticality [Fig. 4(b)]; Refs. [29] assumes antagonistic growth of axons and dendrites and finds criticality, if a certain fraction of neurons becomes inhibitory; Refs. [48, 72, 73] consider more abstract homeostasis and neuron models.

Usually, models for neuronal avalanches only allow to estimate size and duration distributions numerically [14, 25, 27, 29, 30]. Reference [24] obtains an analytical expression of the size distribution for a discrete-time network. Our article derives size and duration distributions for a continuous-time spiking network model after self-organization. These distributions depend only on the experimentally accessible parameters f_0/f_{sat} and τ (duration scaling). The power-law exponents agree with experimentally found ones and those of simple branching processes [4, 6, 8, 14]. The duration distribution has power-law scaling at the tail [4, 6, 14], a fit to short avalanches [8] would yield different results. Our analytical expressions allow fast parameter scans, delineations of the (near-)critical regime and parameter estimations.

From a general perspective, avalanches in our model are clusters of a Hawkes process. While their size distribution can be straightforwardly computed [Eq. (4)], their duration distribution generally requires solving a nonlinear integral equation [58, 59]. Here we show that for Markovian Hawkes processes it follows from the solution of an ordinary differential equation [Eqs. (9),(10)] and we give closed-form approximations. This may find straightforward application in further fields of science where these processes are employed, for example, to characterize durations of financial market fluctuations [57], earthquakes [74], violence [75], and epidemics [76, 77].

[1] D. Marković and C. Gros, Phys. Rep. **536**, 41 (2014), 1310.5527v3.
[2] P. Bak, C. Tang, and K. Wiesenfeld, Phys. Rev. Lett. **59**, 381 (1987).
[3] P. Bak, C. Tang, and K. Wiesenfeld, Phys. Rev. A **38**, 364 (1988).
[4] S. Zapperi, K. B. Lauritsen, and H. E. Stanley, Phys. Rev. Lett. **75**, 4071 (1995), cond-mat/9509161v1.
[5] H. J. Jensen, *Self-Organized Criticality* (Cambridge University Press, Cambridge, 1998).
[6] T. E. Harris, *The Theory of Branching Processes* (Courier, New York, 2002).
[7] S. di Santo, P. Villegas, R. Burioni, and M. A. Muñoz, Phys. Rev. E **95**, 032115 (2017), 1612.07183v3.
[8] J. Beggs and D. Plenz, J. Neurosci. **23**, 11167 (2003).
[9] J. Beggs and D. Plenz, J. Neurosci. **24**, 5216 (2004).
[10] C. Haldeman and J. M. Beggs, Phys. Rev. Lett. **94**, 058101 (2005).
[11] W. L. Shew and D. Plenz, The Neuroscientist **19**, 88 (2013).
[12] A. Mazzoni, F. Broccard, E. Garcia-Perez, P. Bonifazi, M. Ruaro, and V. Torre, PLoS One **2**, e439 (2007).
[13] E. G. Gireesh and D. Plenz, Proc. Natl. Acad. Sci. U.S.A. **105**, 7576 (2008).
[14] M. H. Hennig, C. Adams, D. Willshaw, and E. Sernagor, J. Neurosci. **29**, 1077 (2009).
[15] Y. Yada, T. Mita, A. Sanada, R. Yano, R. Kanzaki, D. J. Bakkum, A. Hierlemann, and H. Takahashi, Neuroscience **343**, 55 (2017).
[16] S. Kater and L. Mills, J. Neurosci. **11**, 891 (1991).
[17] S. Kater, M. Mattson, C. Cohan, and J. Connor, Trends Neurosci. **11**, 315 (1988).
[18] C. Cohan and S. Kater, Science **232**, 1638 (1986).
[19] F. van Huizen and H. Romijn, Brain Res. **408**, 271 (1987).
[20] R. D. Fields, E. A. Neale, and P. G. Nelson, J. Neurosci. **10**, 2950 (1990).
[21] A. van Ooyen, Nat. Rev. Neurosci. **12**, 311 (2011).
[22] G. Turrigiano, Cold Spring Harb. Perspect. Biol. **4**, a005736 (2012).
[23] A. van Ooyen and M. Butz-Ostendorf, *The Rewiring Brain* (Academic Press, London, 2017).
[24] C. W. Eurich, J. M. Herrmann, and U. A. Ernst, Phys. Rev. E **66**, 066137 (2002).
[25] A. Levina, J. M. Herrmann, and T. Geisel, Nat. Phys. **3**, 857 (2007), 0712.1003v1.
[26] A. Levina, J. M. Herrmann, and T. Geisel, Phys. Rev. Lett. **102**, 118110 (2009).
[27] L. Abbott and R. Rohrkemper, Prog. Brain Res. **165**, 13 (2007).
[28] V. Gómez, A. Kaltenbrunner, V. López, and H. J. Kappen, in *Advances in Neural Information Processing Systems 21* (Curran Associates, 2008) pp. 513–520.
[29] C. Tetzlaff, S. Okujeni, U. Egert, F. Wörgötter, and M. Butz, PLoS Comput. Biol. **6**, e1001013 (2010).
[30] B. Del Papa, V. Priesemann, and J. Triesch, PLoS One **12**, e0178683 (2017).
[31] S. Bornholdt and T. Rohlf, Phys. Rev. Lett. **84**, 6114 (2000), cond-mat/0003215v2.
[32] S. Bornholdt and T. Röhl, Phys. Rev. E **67**, 066118 (2003), cond-mat/0109256v2.
[33] C. Meisel and T. Gross, Phys. Rev. E **80**, 061917 (2009), 0903.2987v2.
[34] A. van Ooyen and J. van Pelt, J. Theor. Biol. **167**, 27 (1994).
[35] W. Gerstner and W. Kistler, *Spiking Neuron Models: Single Neurons, Populations, Plasticity* (Cambridge University Press, Cambridge, 2002).

[36] R. Kempter, W. Gerstner, and J. L. Van Hemmen, Phys. Rev. E **59**, 4498 (1999).

[37] A. N. Burkitt, M. Gilson, and J. L. van Hemmen, Biol. Cybern. **96**, 533 (2007).

[38] V. Pernice, B. Staude, S. Cardanobile, and S. Rotter, PLoS Comput. Biol. **7**, e1002059 (2011).

[39] C. Koch, *Biophysics of Computation* (Oxford University Press, Oxford, 1999).

[40] K. J. Ford, A. L. Félix, and M. B. Feller, J. Neurosci. **32**, 850 (2012).

[41] A. G. Hawkes, Biometrika **58**, 83 (1971).

[42] J. Barral and A. Reyes, Nat. Neurosci. **19**, 1690 (2016).

[43] M. Abeles, *Corticonics: Neural Circuits of the Cerebral Cortex* (Cambridge University Press, 1991).

[44] A. van Ooyen, A. Carnell, S. de Ridder, B. Tarigan, H. D. Mansvelder, F. Bijma, M. de Gunst, and J. van Pelt, PLoS One **9**, e85858 (2014).

[45] See Supplemental Material at https://journals.aps.org/prl/supplemental/10.1103/PhysRevLett.121.058301 for further detail, which includes Refs. [46, 47].

[46] S. Johansson and P. Arhem, Proc. Natl. Acad. Sci. U.S.A. **91**, 1761 (1994).

[47] J. Zheng, S. Lee, and Z. Zhou, Nat. Neurosci. **9**, 363 (2006).

[48] J. Zierenberg, J. Wilting, and V. Priesemann, Phys. Rev. X **8** (2018), 10.1103/PhysRevX.8.031018, 1807.01479v1.

[49] K. S. Crump and C. J. Mode, J. Math. Anal. Appl. **24**, 494 (1968).

[50] J. C. Tanner, Biometrika **48**, 222 (1961).

[51] V. Priesemann, M. Wibral, M. Valderrama, R. Pröpper, M. Le Van Quyen, T. Geisel, J. Triesch, D. Nikolić, and M. H. J. Munk, Front. Sys. Neurosci. **8**, 108 (2014).

[52] M. Abramowitz and I. A. Stegun, *Handbook of mathematical functions with formulas, graphs, and mathematical tables* (Dover, New York, 1974).

[53] D. Oakes, J. Appl. Probab. **12**, 69 (1975).

[54] E. Bacry, I. Mastromatteo, and J.-F. Muzy, Mark. Microstruct. Liquidity **1**, 1550005 (2015).

[55] X. Gao and L. Zhu, Stoch. Process. Appl. (2018), 10.1016/j.spa.2017.12.001, 1512.02155.

[56] A. Dassios and H. Zhao, Adv. Appl. Probab. **43**, 814 (2011).

[57] E. Errais, K. Giesecke, and L. R. Goldberg, SIAM J. Finan. Math. **1**, 642 (2010).

[58] A. G. Hawkes and D. Oakes, J. Appl. Probab. **11**, 493 (1974).

[59] J. Møller and J. G. Rasmussen, Adv. Appl. Probab. **37**, 629 (2005).

[60] P. Dayan and L. Abbott, *Theoretical Neuroscience: Computational and Mathematical Modeling of Neural Systems* (MIT Press, Cambridge, 2001).

[61] V. Priesemann, M. H. Munk, and M. Wibral, BMC Neurosci. **10**, 40 (2009).

[62] G. Hahn, T. Petermann, M. N. Havenith, S. Yu, W. Singer, D. Plenz, and D. Nikolic, J. Neurophysiol. **104**, 3312 (2010).

[63] A. Levina and V. Priesemann, Nat. Commun. **8**, 15140 (2017), 1701.04277.

[64] A. Clauset, C. R. Shalizi, and M. E. J. Newman, SIAM Rev. **51**, 661 (2009), 0706.1062v2.

[65] S. V. Aksenov, M. A. Savageau, U. D. Jentschura, J. Becher, G. Soff, and P. J. Mohr, Comput. Phys. Commun. **150**, 1 (2003), math/0207086v1.

[66] Didier Sornette, J. Phys. I France **4**, 209 (1994).

[67] J. A. Bonachela and M. A. Muñoz, J. Stat. Mech. **2009**, P09009 (2009).

[68] J. A. Bonachela, S. De Franciscis, J. J. Torres, and M. A. Muñoz, J. Stat. Mech. **2010**, P02015 (2010).

[69] W. L. Shew, H. Yang, S. Yu, R. Roy, and D. Plenz, J. Neurosci. **31**, 55 (2011).

[70] T. Vogels and L. Abbott, J. Neurosci. **25**, 10786 (2005).

[71] A. Kumar, S. Schrader, A. Aertsen, and S. Rotter, Neural Comput. **20**, 1 (2008).

[72] A. Levina, U. Ernst, and J. M. Herrmann, Neurocomputing **70**, 1877 (2007).

[73] F. Droste, A.-L. Do, and T. Gross, J. Royal Soc. Interface **10**, 20120558 (2013), 1203.4942v2.

[74] T. Wang, M. Bebbington, and D. Harte, Ann. Inst. Stat. Math. **64**, 521 (2012).

[75] E. Lewis, G. Mohler, P. J. Brantingham, and A. L. Bertozzi, Secur. J. **25**, 244 (2012).

[76] H. Kim, *Spatio-Temporal Point Process Models for the Spread of Avian Influenza Virus (H5N1)*, Ph.D. thesis (2011).

[77] F. Schoenberg, M. Hoffmann, and R. Harrigan, arXiv:1703.08202 [stat.ME].

Growing Critical: Self-Organized Criticality in a Developing Neural System
– Supplemental Material –

Felipe Yaroslav Kalle Kossio,[1] Sven Goedeke,[1] Benjamin van
den Akker,[2] Borja Ibarz,[3] and Raoul-Martin Memmesheimer[1,2]

[1]*Neural Network Dynamics and Computation,*
Institute of Genetics, University of Bonn, Bonn, Germany

[2]*Department of Neuroinformatics, Radboud University Nijmegen, Nijmegen, Netherlands*

[3]*Nonlinear Dynamics and Chaos Group, Departamento de Fisica,*
Universidad Rey Juan Carlos, Madrid, Spain

I. MANIPULATION OF NEURAL EXCITABILITY

To address the impact of a typical experimental manipulation on the dynamics of our networks, we change the neural excitability or, equivalently, the coupling strength via g. We find that after decreasing it, in the short term activity is subcritical, Figs. S1(a), S2(a). The neurites react to the resulting overall loss of input by outgrowth, which leads to strengthening of connections and finally to the recovery of the near-critical state. An increase of neural excitability leads to very strong activity, which is quickly overcompensated by a decrease of connection strengths within the course of a single large avalanche, Fig. S1(c). The system becomes subcritical and regains the near-critical state more slowly thereafter. In biological neural networks overly large spiking activity is prevented by refractoriness. When decreasing neural excitability, our network models incorporating refractoriness behave similar to those without, Figs. S1(b), S2(b). When increasing excitability, in the short term they display an excess of medium size and large avalanches, Fig. S2(c). The overlap sizes and coupling strengths decrease until the near-critical state is regained, Fig. S1(d). This happens faster than the adaptation from subcriticality due to the still large excess of spiking: in Fig. S2(c) the distribution in green is already similar to that in gray, in Fig. S2(a,b) the distributions in blue are markedly different from those in gray.

In agreement with our findings, experimental studies have shown that a global decrease of excitatory synaptic strengths (decrease of network excitability) leads to subcritical activity while a global decrease of inhibitory synaptic strengths (increase of network excitability) leads to supercritical behavior with an excess of large avalanches [1, 2].

II. ROBUSTNESS OF AVALANCHE CHARACTERISTICS AGAINST CHANGES IN THE SPONTANEOUS AND SATURATION SPIKE RATES

The stationary state avalanche size and duration distributions are largely independent of the choice of f_0 and f_{sat}, Fig. S3. They are practically critical whenever f_0 is small against f_{sat}. For all finite values of f_{sat} and non-zero values of f_0 there is ultimately an exponential cutoff, see Eq. (5) and Eqs. (9), (10) after expanding around $a(t) = 0$. The large range parameter scans in Fig. S3 are greatly facilitated by our analytical formulas: They allow us to efficiently determine the avalanche characteristics for the markedly subcritical as well as for the near-critical regime, where usually long numerical simulations are necessary to capture the distribution tails with their large and long avalanches. For illustration, Fig. S3 exemplarily highlights the results for the parameters used in Fig. 3 as well as for parameter sets where f_{sat} is multiplied or divided by two (red, green, distributions are near-critical), or f_0 is increased by a factor of 50 (orange, distribution is markedly subcritical).
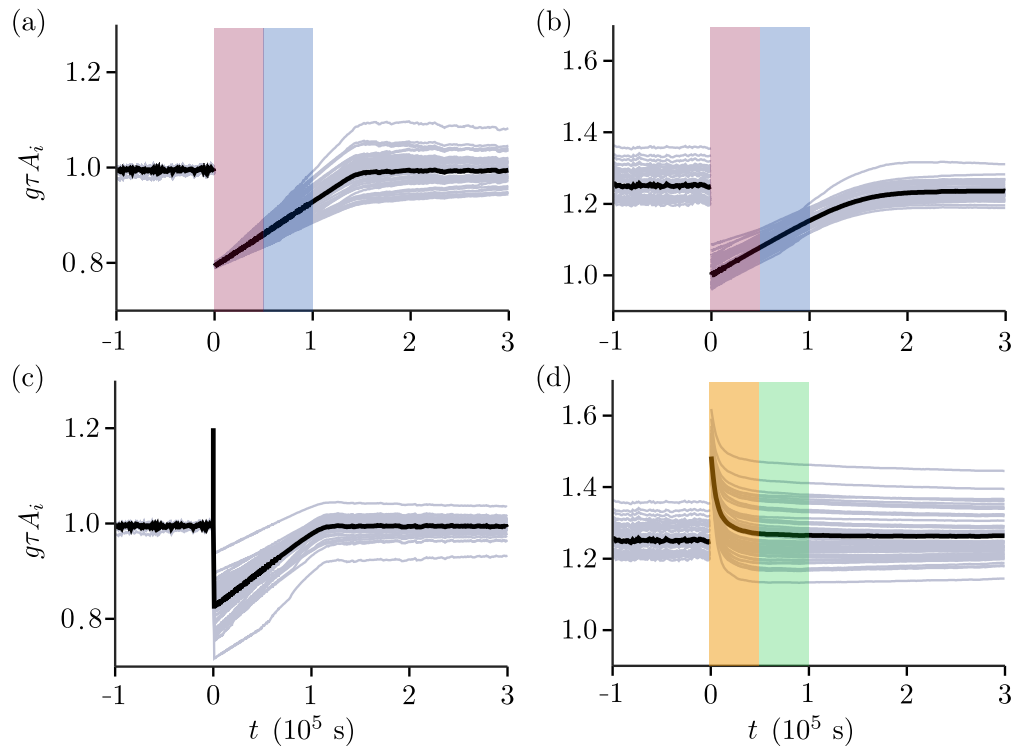
Figure S1. Coupling strengths after manipulation of neural excitability. Scaled total overlaps of 50 neurons (gray) and mean total overlap (black), similar to Fig. 2(c). At $t = 0\,\text{s}$, the excitability g of all neurons is decreased, $g \to 0.8g$ (a,b), or increased, $g \to 1.2g$ (c,d). Before, the networks are in a stationary state. Neurons in (b,d) have refractory period $\tau_{\text{ref}} = \tau$. Avalanche size distributions for the color shaded areas are displayed in Fig. S2 (sampling time $0.5 \times 10^5\,\text{s}$ each). The network growth rate is set to $K^{-1} = 2 \times 10^7\,\text{s}$ prior to manipulation to allow longer sampling times.

Values of f_0 and f_{sat} were directly measured in neural systems generating neuronal avalanches. The findings confirm that our assumption of $f_0/f_{\text{sat}} \ll 1$ is justified: Ref. [3] measures spike rates in retinal starburst amacrine cells in isolation and embedded in their network, where critical avalanches were reported a few days after birth [5]. The study finds spontaneous spike rates of isolated neurons that decrease from $f_0 \approx 1.3\,\text{mHz}$ to $f_0 \approx 0.1\,\text{mHz}$ between postnatal day 2 and postnatal day 6, Fig. 1 in Ref. [3]. The average spike rate $\bar{f} \approx 13\,\text{mHz}$ of connected neurons stays constant; we may assume $f_{\text{sat}} \approx 13\,\text{mHz}$ (or higher, if the homeostatic network plasticity is slow). The ratio f_0/f_{sat} therefore decreases from $f_0/f_{\text{sat}} \approx 0.1$ to $f_0/f_{\text{sat}} \approx 0.01$, Fig. S3, cyan. Reference [4] investigates avalanches in neuronal cultures. The study reports a population spike rate, which rises from approximately $45\,\text{Hz}$ at day 4 in vitro to approximately $730\,\text{Hz}$ at day 30 in vitro, Fig. 5 in Ref. [4]. The first value is an upper estimate for $f_0 \times N$, where N is the number of neurons recorded from. The estimate neglects already existing couplings and mutual excitation between neurons after four days. The second value is a lower estimate for $f_{\text{sat}} \times N$, since the networks may grow further. We thus have $f_0 < 45\,\text{Hz}/N$ and $f_{\text{sat}} > 730\,\text{Hz}/N$, such that $f_0/f_{\text{sat}} < 0.06$, Fig. S3, pink line.
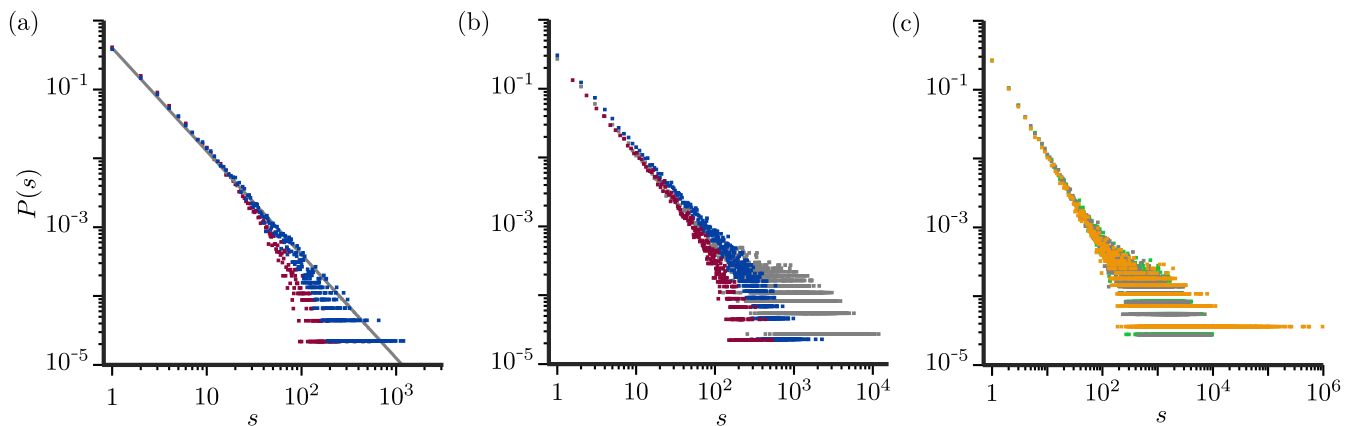
Figure S2. Avalanche size distributions after manipulation of neural excitability. (a) Network of Fig. S1(a). Red and blue: distributions sampled directly after decreasing excitability [Fig. S1(a), red shading] and in the subsequent interval [Fig. S1(a), blue shading], respectively. Gray: analytical stationary state distribution Eq. (4). (b) Like (a) for the network of Fig. S1(b). Gray: stationary state distribution (sampled from simulation). (c) Network of Fig. S1(d). Orange: distribution sampled directly after increasing excitability [Fig. S1(d), orange shading]. Green: distribution sampled during the subsequent interval [Fig. S1(d), green shading]. Gray: stationary state distribution.

III. INDEPENDENCE OF AVALANCHE CHARACTERISTICS OF OTHER MODEL PARAMETERS

Equation (4) shows that the stationary state avalanche size distribution only depends on f_0 and f_{sat} (via $\sigma = 1 - f_0/f_{\text{sat}}$). Similarly, Eqs. (9), (10) show that the duration distribution depends only on f_0, f_{sat}, and τ. Equation (6) implies that changing τ is equivalent to rescaling the time axis and therefore only leads to a rescaling of the duration distribution. The dependence of avalanche statistics on the other model parameters, which do not enter Eqs. (4), (9), and (10), such as the coupling parameter g, the number of neurons N, the growth rate K, the dimensions of the square where the neurons are placed, and the way they are placed in (regular vs. random) vanishes during the network's self-organization process.

Consider as an example the coupling parameter g: If g is small, the network growth leads to larger total overlaps involving more synaptic partners. If g is large, the network growth leads to smaller total overlaps involving fewer synaptic partners. In the end, the dynamics are near-critical irrespective of g's value, Fig. S4. The value of g may thus be chosen according to the biological system to which our model is applied. Indeed, ranges of overlaps and numbers of synaptic connection partners differ widely in full grown networks of potential relevance for our model: Neurons in cultures establish connections to tens and hundreds of other neurons, depending on the density of the plating [6], starburst amacrine cells receive inputs from tens of other starburst amacrine cells [5, 7], and in the intact cortex, neurons have thousands of different neurons as synaptic partners [8].
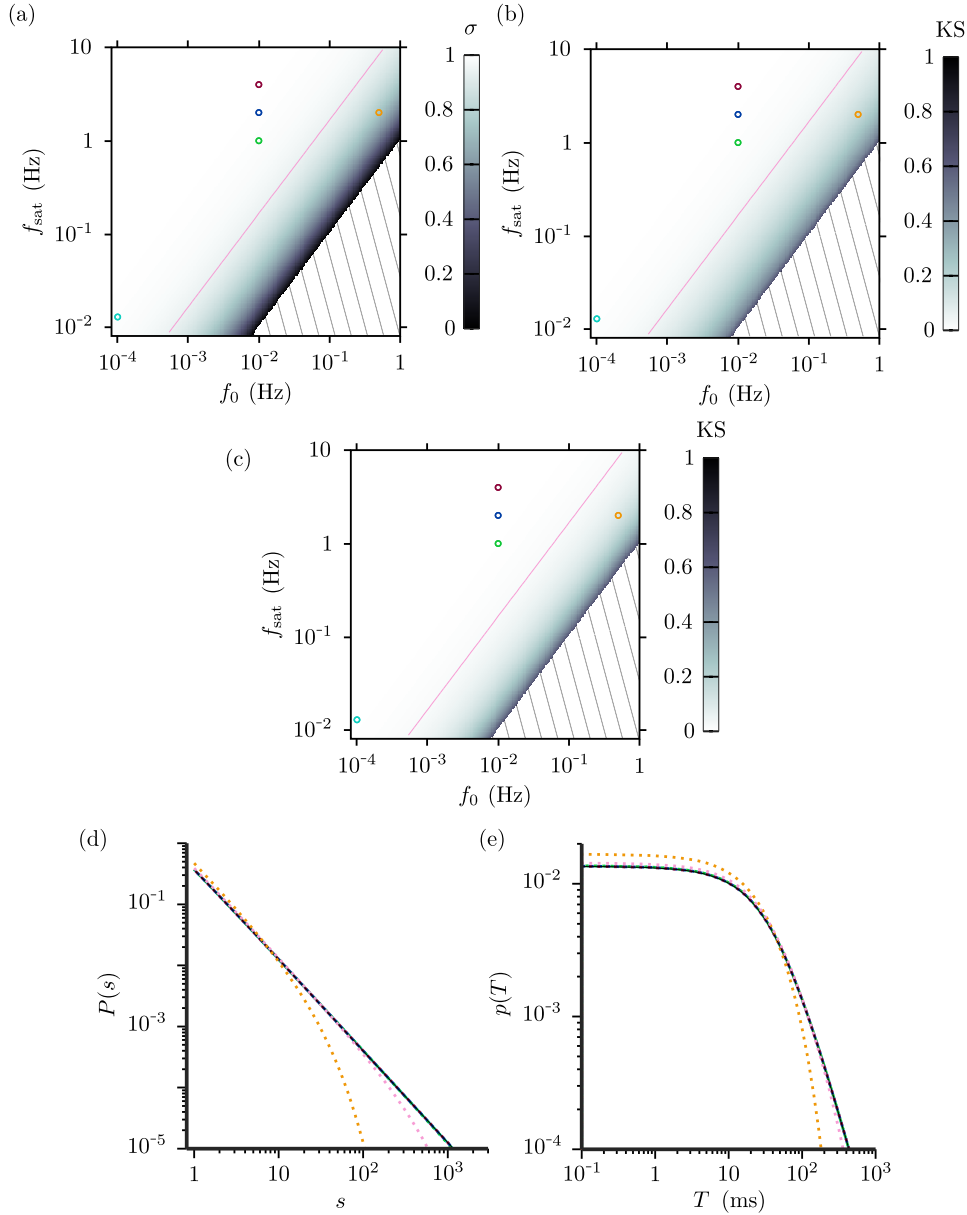
Figure S3. Stationary state avalanche size and duration distributions are near-critical for large ranges of f_{sat} and f_0. (a) Branching parameter σ (gray scale, hatched area: $\sigma < 0$, system undefined) of the stationary state dynamics as a function of f_0 and f_{sat}. σ is close to 1 for large ranges of f_{sat} and f_0. (b) Kolmogorov-Smirnov distance (KS) between the critical size distribution [Eq. (4), $\sigma = 1$] and distributions with different f_{sat} and f_0 [Eq. (4), $\sigma = 1 - f_0/f_{\text{sat}}$]. The distance is close to 0 for large ranges of f_{sat} and f_0. (c) Like (b) for the avalanche duration distributions Eqs. (9), (10). KS is close to 0 for large ranges of f_{sat} and f_0. Circles: $f_{\text{sat}} = 2\,\text{Hz}$, $f_0 = 0.01\,\text{Hz}$ (blue, $\sigma = 0.995$, used in the main text), $f_{\text{sat}} = 4\,\text{Hz}$, $f_0 = 0.01\,\text{Hz}$ (red, $\sigma = 0.9975$), $f_{\text{sat}} = 1\,\text{Hz}$, $f_0 = 0.01\,\text{Hz}$ (green, $\sigma = 0.99$), $f_{\text{sat}} = 13\,\text{mHz}$, $f_0 = 0.1\,\text{mHz}$ (cyan, $\sigma = 0.9923$) [3], $f_{\text{sat}} = 2\,\text{Hz}$, $f_0 = 0.5\,\text{Hz}$ (orange, $\sigma = 0.75$); pink line: $f_0/f_{\text{sat}} = 0.06$, upper limit of the ratio derived from Ref. [4] ($\sigma = 0.94$). (d,e) Size and duration distributions for the parameter values highlighted in (a-c) in alike colors (dotted for better discrimination, $\tau = 10\,\text{ms}$). The distributions in red, blue, green, cyan, and pink are near-critical, they partially overlay each other and the critical distributions (black). The distributions in orange are subcritical.
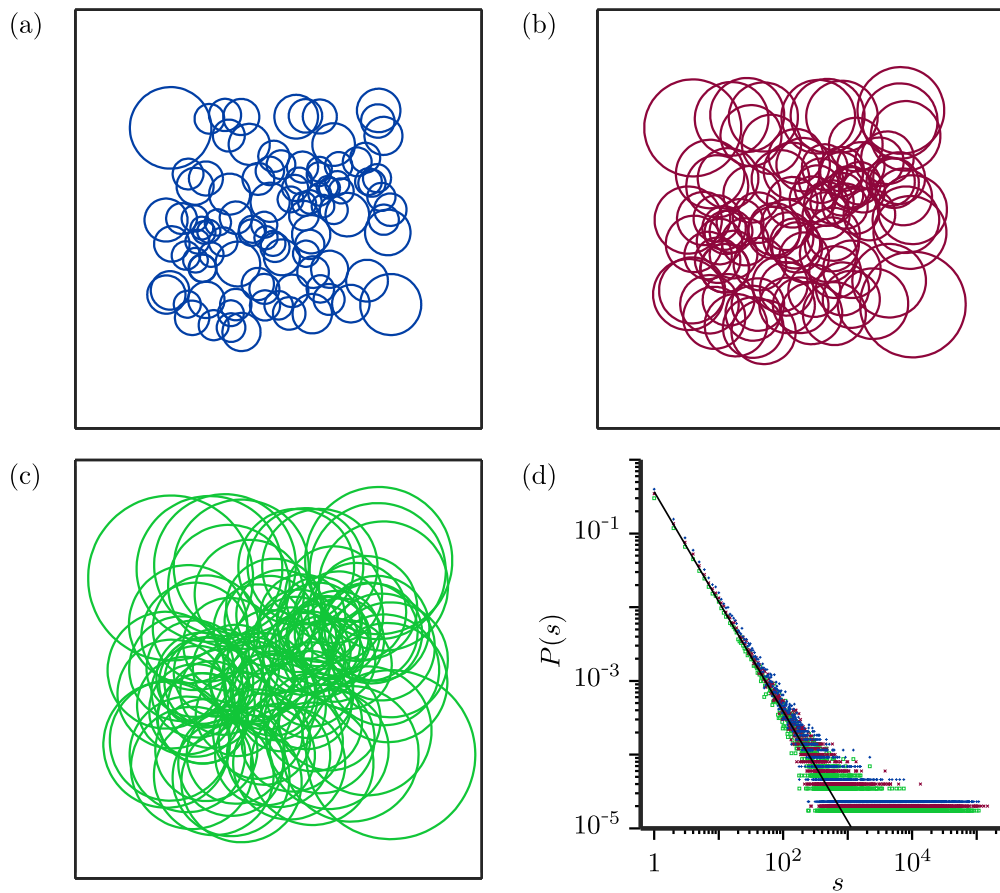
Figure S4. The choice of the parameter g does not influence the avalanche statistics in the stationary state. (a), (b), and (c) display networks of $N = 100$ neurons in the stationary state for $g = 5\,\text{kHz}$, $g = 500\,\text{Hz}$, and $g = 50\,\text{Hz}$, respectively. (d) shows that the avalanche size distributions of these networks agree [networks in (a), (b), (c): blue +, red x, green squares]. Distributions are slightly vertically shifted for better discriminability.

IV. SPONTANEOUSLY ACTIVE SUBPOPULATION

The stationary state avalanche size and duration distributions in our model are unchanged, if only a subpopulation of neurons is spontaneously active [9]. The quantity f_0 relevant for the statistics is the average spontaneous activity per neuron, see Fig. S5. The size of the spontaneously active subpopulation may be small against N, which leads to an f_0 that is small against the individual spontaneous rates.

V. BINNING

We choose the bin size such that it keeps analytical probability estimates for different errors that are generated by binning moderate, Fig. S6. The considered errors are: (i) joining the initial spike of an avalanche to the next avalanche, (ii) splitting the first spikes of the same avalanche, (iii) joining an average
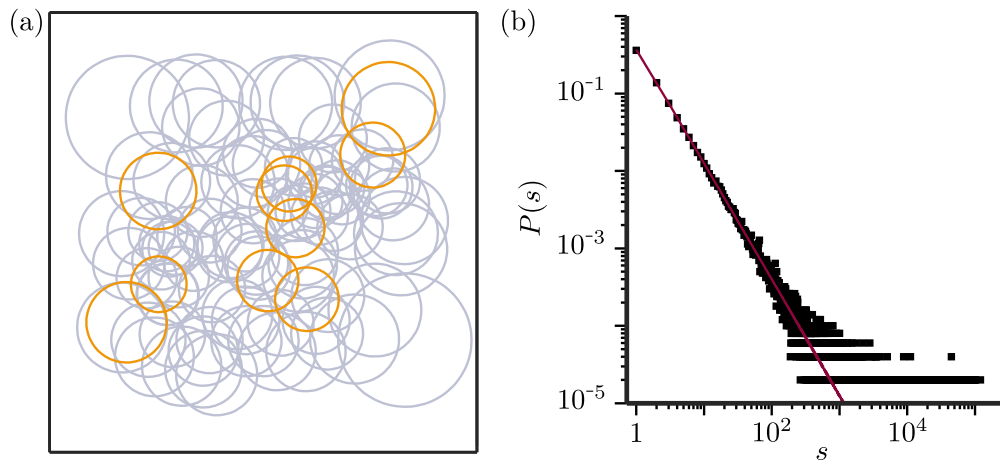
Figure S5. Avalanche statistics in the stationary state are unchanged, if only a subpopulation of neurons is spontaneously active. (a) Network of neurons in the stationary state with 10 out of 100 neurons spontaneously active with rate $\tilde{f}_0 = 0.1\,\text{Hz}$ (orange). (b) The network's avalanche size distribution (numerically estimated, black) agrees with that of a network where all neurons are spontaneously active with $f_0 = 0.1\tilde{f}_0$ [Eq. (4), red].

size avalanche to the next one, and (iv) splitting an average size avalanche. The resulting bin size t_{bin} depends on f_0, τ, N, and f_{sat}, which are experimentally accessible from single neuron measurements, anatomical data, and averaged spiking activity.

We first compute a simple estimate for the probability that binning joins the initial spontaneous progenitor spike of an avalanche to the next avalanche. Thereafter, we compute an estimate for the probability of splitting an avalanche between its first two spikes. These two probabilities yield a lower estimate for the probabilities of splitting and joining avalanches, as avalanches extending beyond their initial or first two spikes have higher probabilities of being joined to the next or being split. Keeping the obtained probabilities small provides an indication for an appropriate bin size, in particular because small avalanches are frequent. To compute the probability of joining the first spike of an avalanche to the next avalanche, we use that the rate of spontaneous progenitor spikes in the network is Nf_0. The interspike-interval (ISI) distribution of spontaneous spikes is therefore $p_{\text{ISI}}(t) = Nf_0 e^{-Nf_0 t}$. The probability of joining the initial spike of an avalanche to the following initial spike of an avalanche is approximately (the bin will usually not start at the first avalanche's start) the probability that the ISI between progenitor spikes is less than t_{bin},

$$P(\text{join first}) \approx \int_0^{t_{\text{bin}}} p_{\text{ISI}}(t)dt = 1 - e^{-Nf_0 t_{\text{bin}}}. \tag{S1}$$

We now estimate the probability of splitting the first two spikes of an avalanche. This is approximately the probability that the second spike of the avalanche will occur more than t_{bin} apart from the first, $P(\text{split first}) \approx P(t_{\text{bin}} < t_2 < \infty)$, where t_2 is time of the second spike. The first spike increases the firing
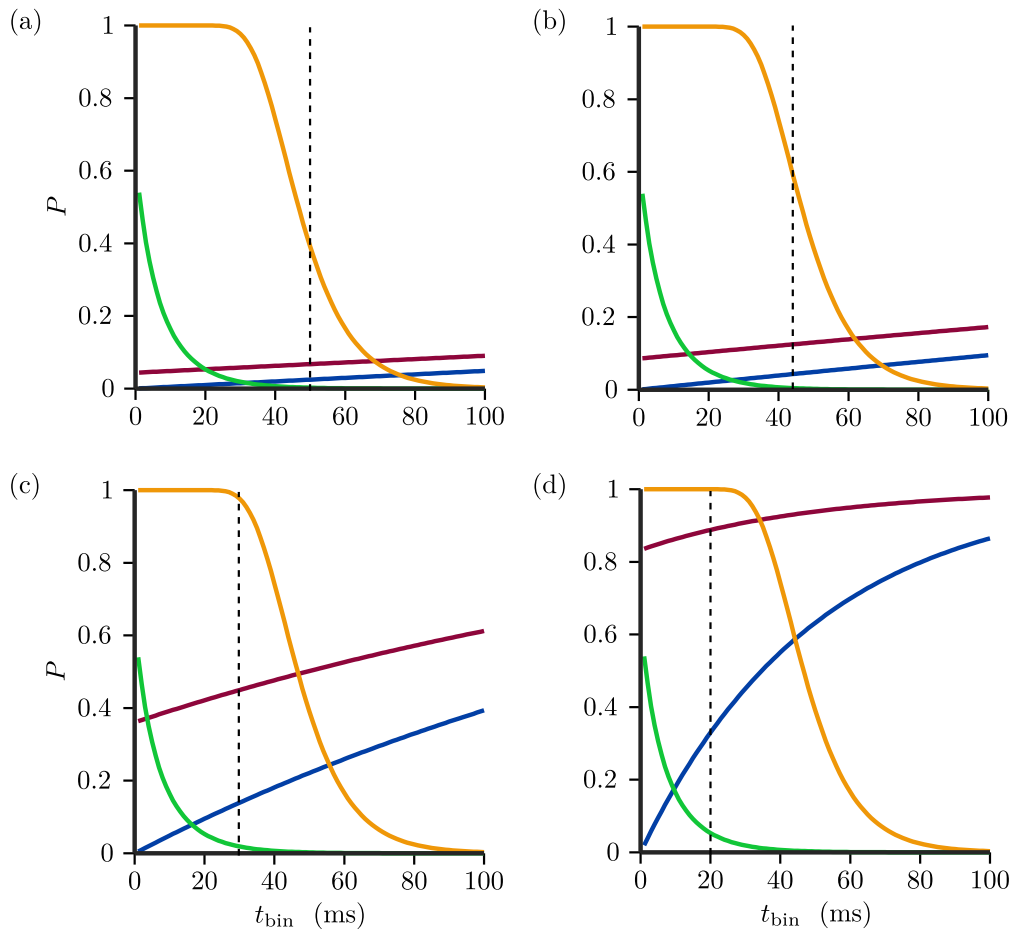
Figure S6. Probability estimates for joining and splitting of avalanches for networks of (a) $N = 50$, (b) $N = 100$, (c) $N = 500$, (d) $N = 2000$ neurons and $\tau = 10\,\mathrm{ms}$, $f_0 = 0.01\,\mathrm{Hz}$, $f_{\mathrm{sat}} = 2\,\mathrm{Hz}$. Each panel displays our estimates for joining and splitting first spikes and average avalanches $P(\mathrm{join\ first})$ Eq. (S1) (blue), $P(\mathrm{split\ first})$ Eq. (S4) (green), $P(\mathrm{join\ average})$ Eq. (S5) (magenta), and $P(\mathrm{split\ average})$ Eq. (S6) (orange) versus bin size. The dashed line in (b) indicates the bin size chosen for the data analysis in Figs. 3, 4, S2, S4, and S5; the other dashed lines indicate suitable bin sizes for other network sizes.

rate of the system by σ/τ, so $P(\mathrm{split\ first})$ can be written as

$$P(\mathrm{split\ first}) \approx P(t_{\mathrm{bin}} < t_2 < \infty) = P(t_{\mathrm{bin}} < t_2) - P(t_2 = \infty) \tag{S2}$$

$$= e^{-\int_0^{t_{\mathrm{bin}}} \frac{\sigma}{\tau} e^{-t/\tau} dt} - e^{-\int_0^{\infty} \frac{\sigma}{\tau} e^{-t/\tau} dt} \tag{S3}$$

$$= e^{-\sigma(1-e^{t_{\mathrm{bin}}/\tau})} - e^{-\sigma}. \tag{S4}$$

To assess how to choose the bin size to keep probabilities of joining and splitting larger avalanches moderate as well, we derive similar estimates for avalanches with average length and duration. The probability of joining an avalanche of average duration $\bar{T}$ to the next one is approximately

$$P(\mathrm{join\ average}) \approx \int_0^{\bar{T}+t_{\mathrm{bin}}} p_{\mathrm{ISI}}(t)dt = 1 - e^{-Nf_0(\bar{T}+t_{\mathrm{bin}})}; \tag{S5}$$
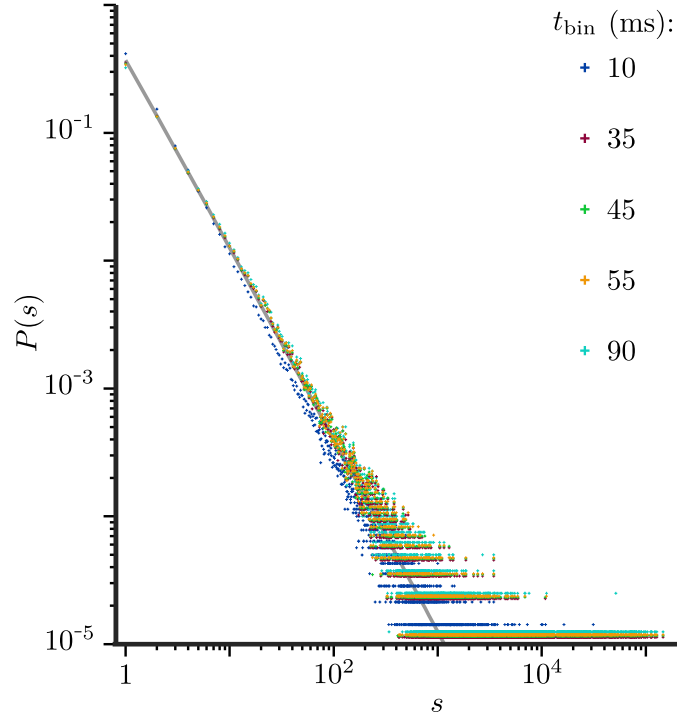
Figure S7. Robustness against large changes in bin size. The figure displays avalanche size distributions obtained using bin sizes $t_{\text{bin}} = 10\,\text{ms}$ (blue), $t_{\text{bin}} = 35\,\text{ms}$ (red), $t_{\text{bin}} = 45\,\text{ms}$ (green), $t_{\text{bin}} = 55\,\text{ms}$ (orange), and $t_{\text{bin}} = 90\,\text{ms}$ (cyan). The distributions obtained with $t_{\text{bin}} = 35\,\text{ms}$, $t_{\text{bin}} = 45\,\text{ms}$, $t_{\text{bin}} = 55\,\text{ms}$, and $t_{\text{bin}} = 90\,\text{ms}$ are similar, the one obtained with $t_{\text{bin}} = 10\,\text{ms}$ deviates, as expected from Fig. S6(b). The analyzed spike data are generated by a network with our standard parameters $N = 100$, $\tau = 10\,\text{ms}$, $f_0 = 0.01\,\text{Hz}$, $f_{\text{sat}} = 2\,\text{Hz}$; we usually use $t_{\text{bin}} = 45\,\text{ms}$ for such data, Fig. S6(b).

we compute $\bar{T}$ by numerically integrating $\bar{T} = \int_{0^-}^{\infty} T p(T) dT$, where $p(T)$ is given by Eq. (10). To estimate the probability of splitting an avalanche of approximately average size $\bar{s} = 1/(1-\sigma)$ [mean of the Borel distributed avalanche size, Eq. (4)], we first note that the split may occur about $\bar{s} - 1 = \sigma/(1-\sigma)$ times, which is the average number of offspring spikes in the branching process. We assume that the excitation from the previous avalanche spike has decayed to nearly zero when another one occurs, such that the next spike is generated by the previous only. Each spike of the avalanche then increases the collective firing rate to about σ/τ above the level of spontaneous spiking, like a progenitor spike. Since this implies that interspike-intervals are long, our assumption is conservative and gives us a higher probability to split the avalanche. It allows us to employ the already derived $P(\text{split first})$ as an estimate for splitting one of the $\sigma/(1-\sigma)$ intervals between avalanche spikes. The probability of not splitting an average size avalanche is approximately $(1 - P(\text{split first}))^{\sigma/(1-\sigma)}$ and thus

$$P(\text{split average}) \approx 1 - (1 - P(\text{split first}))^{\frac{\sigma}{1-\sigma}} \approx 1 - \left(1 - e^{-\sigma(1-e^{t_{\text{bin}}/\tau})} - e^{-\sigma}\right)^{\frac{\sigma}{1-\sigma}}. \qquad \text{(S6)}$$

Replacing P(split first) by the probability of splitting an avalanche of two spikes yields similar results.

Figure S6 displays the four probabilities Eqs. (S1), (S4), (S5), and (S6) against bin size. For small bin size there is a high probability of splitting an avalanche, which would result in overestimating the decay of avalanche distributions and possible critical exponents. The probability of splitting an avalanche becomes negligible for large bin size. For large bin size, however, there is a high probability of joining avalanches, which would result in underestimating the decay of avalanche distributions and possible critical exponents. Our above estimates allow us to choose a bin size in between. For a faithful detection of the avalanche characteristics, it is more important to avoid joining small avalanches and splitting initial avalanche spikes, since they are most frequent. The bin size should thus be chosen such that keeping the probabilities P(join first) and P(split first) small is attributed a higher weight than keeping the probabilities P(join average) and P(split average) small. For the binning of our numerical data, we thus choose a bin size in the middle of the interval delimited by the crossings of P(join first) and P(split first) on the left and P(join average) and P(split average) on the right.

Our results are not sensitive to the chosen bin size. Since the time scales of avalanche dynamics and avalanche generation are well separated, most avalanches are relatively short and far apart, so the probability to join two avalanches increases slowly with bin size and there is a large range of suitable ones, see Fig. S7.

[1] J. Beggs and D. Plenz, J. Neurosci. **23**, 11167 (2003).

[2] W. L. Shew, H. Yang, S. Yu, R. Roy, and D. Plenz, J. Neurosci. **31**, 55 (2011).

[3] K. J. Ford, A. L. Félix, and M. B. Feller, J. Neurosci. **32**, 850 (2012).

[4] Y. Yada, T. Mita, A. Sanada, R. Yano, R. Kanzaki, D. J. Bakkum, A. Hierlemann, and H. Takahashi, Neuroscience **343**, 55 (2017).

[5] M. H. Hennig, C. Adams, D. Willshaw, and E. Sernagor, J. Neurosci. **29**, 1077 (2009).

[6] J. Barral and A. Reyes, Nat. Neurosci. **19**, 1690 (2016).

[7] J. Zheng, S. Lee, and Z. Zhou, Nat. Neurosci. **9**, 363 (2006).

[8] M. Abeles, *Corticonics: Neural Circuits of the Cerebral Cortex* (Cambridge University Press, 1991).

[9] S. Johansson and P. Arhem, Proc. Natl. Acad. Sci. U.S.A. **91**, 1761 (1994).